Role of electron-phonon interaction in a magnetically driven mechanism for superconductivity

H. Bakrim and C. Bourbonnais

Regroupement Québecois sur les Matériaux de Pointe, Département de physique, Université de Sherbrooke, Sherbrooke, Québec, Canada J1K-2R1

(Received 24 June 2014; revised manuscript received 28 August 2014; published 9 September 2014)

We use the renormalization group method to examine the effect of phonon-mediated interaction on d-wave superconductivity, as driven by spin fluctuations in a quasi-one-dimensional electron system. The influence of a tight-binding electron-phonon interaction on the spin-density-wave and d-wave superconducting instability lines is calculated for arbitrary temperature, phonon frequency, and antinesting of the Fermi surface. The domain of electron-phonon coupling strength where spin-density-wave order becomes unstable against the formation of a bond-order wave or Peierls state is determined at weak antinesting. We show the existence of a positive isotope effect for spin-density-wave and d-wave superconducting critical temperatures which scales with the antinesting distance from quantum critical point where the two instabilities merge. We single out a low phonon frequency zone where the bond-order-wave ordering gives rise to triplet f-wave superconductivity under nesting alteration, with both orderings displaying a negative isotope effect. We also study the electron-phonon strengthening of spin fluctuations at the origin of extended quantum criticality in the metallic phase above superconductivity. The impact of our results on quasi-one-dimensional organic conductors like the Bechgaard salts where a Peierls distortion is absent and superconductivity emerges near a spin-density-wave state under pressure is emphasized.

DOI: 10.1103/PhysRevB.90.125119 PACS number(s): 74.70.Kn, 74.20.Mn, 75.30.Fv, 71.45.Lr

I. INTRODUCTION

The role of electron-phonon coupling in strongly correlated electron systems is an issue of growing importance in materials where unconventional superconductivity is found to compete with various forms of electronic states [1–3]. A point at issue in the quest of understanding the origin of superconductivity is the extend to which the electron-phonon interaction can influence and even modify the nature of Cooper pairing when electrons are strongly correlated, especially through magnetism. In this work we shall focus on this issue in quasi-one-dimensional molecular superconductors where superconductivity takes place in the close proximity of antiferromagnetism, as best exemplified in the Bechgaard salts series of organic superconductors [4].

Since the discovery of superconductivity (SC) in the Bechgaard salts [$(TMTSF)_2X$] series [5], much of the attention paid to the mechanism of Cooper pairing has mostly focused on models of electrons with purely repulsive interactions [4,6–16]. On empirical grounds, this has been amply supported by the ubiquity of spin-density-wave (SDW) correlations near the superconducting state when pressure [17–20], temperature [21,22], or even magnetic field is varied [23,24]. As one moves along the temperature axis, for example, and enters the metallic state, important SDW fluctuations are found to govern properties of the normal phase, giving rise, for instance, to a huge enhancement of the NMR spin relaxation rate and to linear-T resistivity term over a wide temperature interval above the critical temperature T_c for superconductivity [20,22,25].

Besides the nesting of the Fermi surface, repulsive interactions are an essential component of SDW correlations [6,26–28]. They have become inescapable ingredients of the model description of superconductivity in these materials. In this regard, the quasi-one-dimensional electron gas model with the aid of the renormalization group (RG) method have played an important part in the description of these low-dimensional electron systems. In the repulsive sector, it proved particularly generic of the SDW-to-d-wave SC (SC-d) sequence of instabilities when the amplitude of the next-to-nearest neighbor interchain hopping, $t'_\perp$, called the antinesting parameter, is tuned to simulate pressure effects on spin fluctuations responsible for superconducting pairing interaction [29,30]. The approach has also shown how the constructive interference between spin fluctuations and Cooper pairing can explain the existence of a Curie-Weiss temperature dependence of the SDW correlation length, which is a key factor in the enhancement of the NMR relaxation rate and the linear-T component in resistivity over the whole pressure interval where superconductivity is present [20,31–33].

However, in view of the complex molecular structure of systems like the Bechgaard salts, the repulsive electron gas model must be regarded as an idealization. It ignores primarily the interaction of electrons with low-energy phonon modes of the lattice. Early x-ray diffuse scattering experiments in $(TMTSF)_2PF_6$ and $(TMTSF)_2ClO_4$ compounds did reveal the existence of such a coupling, under the guise of lattice fluctuations at the one-dimensional (1D) wave vector $2k_F$ of the electron gas (k_F being the longitudinal Fermi wave vector) [34,35]. The lattice fluctuations remain regular in temperature for the Bechgaard salts, in contrast to so many molecular chain systems where it terminates in a Peierls [bond-order-wave (BOW)] distorted state. Although the reason for this remains largely unexplained [35,36], the presence of $2k_F$ lattice fluctuations is direct evidence of a finite (momentum-dependent) coupling between electrons and phonons, a consequence of the modulation of tight-binding electron band parameters by lattice vibrations.

This points at the impact a retarded [phonon-mediated (Ph-M)] interaction of that kind can have on the properties of the electron gas when the mechanism for Cooper pairing is magnetically driven. Whether it is detrimental to SDW and SC-d correlations, as one would naturally expect if the electron-phonon interaction was taken in isolation [37], or, on the contrary, if it becomes a factor of reinforcement when it is subordinate to repulsive interactions is an open question. The

latter possibility can provide new insight as to the conditions prevailing in weakly dimerized systems like the Bechgaard salts that make SDW predominate over the Peierls phenomena.

More generically, it can clarify how a momentum-dependent electron-phonon interaction can be actively involved in the occurrence of superconductivity near magnetism. It can also shed light on the possibility of a positive isotope effect for the temperature scale of instabilities against SDW and SC-d orderings as a function of phonon frequency. Reinforcement could also extend relatively far in the metallic phase by enhancing spin fluctuations as quantum critical effects due to interfering SC-d and SDW instabilities [32].

These possibilities are important in the context of other unconventional superconductors, in particular high-T_c cuprates [38–41], where they framed a significant part of the debate surrounding the relative importance of Coulomb and electron-phonon interactions when superconductivity takes place in the proximity of antiferromagnetism [1,42–50] and charge-density-wave ordering [51,52]. Its transposition in quasi-one-dimensional superconductors like the Bechgaard salts close to a SDW instability has remained essentially unexplored since the very first attempts to reconcile electron-electron and electron-phonon interactions in the framework of mean-field theory of competing magnetism and superconductivity [27].

In this work we shall address this problem in the weak-coupling framework of the RG approach to the quasi-1D electron gas model. The model is extended to include both direct and momentum-dependent Ph-M electron-electron interactions in the the study of interfering (electron-electron) Cooper and (electron-hole) density-wave pairings at arbitrary phonon frequency ω_D. The RG calculations will be carried out at finite temperature T, which brings additional difficulties in the presence of retarded interactions. This turns out to be required when antinesting is present. Actually, a finite $t'_\perp$ breaks the usual correspondence between T and the scaled cut-off energy $\Lambda(\ell)$ from the Fermi surface that generates the RG flow. The flow will be then conducted at arbitrary temperature for interactions with momentum dependence along the Fermi surface and a finite set of Matsubara frequencies. This finite-T RG procedure with momentum and frequency variables has been worked out recently for systems where Ph-M interactions are predominant, a situation relevant to competing charge-density-wave and s-wave SC instabilities away from half-filling [37]. It is extended here to weakly dimerized chains systems like the Bechgaard salts where repulsive interactions are dominant and half-filling Umklapp scattering is finite [6,31,32].

The results put forward below show that the modulation of tight-binding electron band by acoustic lattice vibrations introduces effective Ph-M interactions with a very characteristic dependence on longitudinal electron momentum and momentum transfer of scattered electrons. The dependence affects the RG flow and produces a low-energy downward screening of the repulsive backward scattering and an enhancement of both repulsive forward and Umklapp scattering terms. These effects are ω_D dependent, concurring to boost antiferromagnetic exchange between itinerant electrons which primarily reinforces the SDW instability line and in turn the magnetically driven SC-d in the phase diagram. The impact of retardation generates a positive isotope effect whose amplitude peaks at the critical strength of antinesting where SDW and SC-d instabilities lines meet and their constructive interference is the strongest. Above a definite strength of electron-phonon interaction, the SDW becomes unstable against the formation of a BOW distorted state and triplet f-wave superconductivity if antinesting and retardation are sufficiently high. The latter states are both characterized by a negative isotope effect, as a result of antiadiabaticity.

The boost of exchange by electron-phonon interaction is not limited to the transition lines but is manifest in the metallic phase where it feeds deviations to Fermi liquid behavior at the origin of extended quantum criticality in the normal phase [20,31,32]. The latter can be followed through the reinforcement of the Curie-Weiss behavior of the SDW susceptibility which is correlated to ω_D and antinesting $t'_\perp$ in the whole range where superconductivity is present.

In Sec. II we introduce the quasi-1D electron gas model which is extended to include the tight-binding electron-phonon interaction term. In Sec. III the one-loop RG flow equations for the different electron-electron vertices and relevant response functions are given and integrated into the determination of the phase diagram at arbitrary antinesting and phonon frequency. Their integration is carried out in Sec. IV and leads to the determination of the phase diagrams, isotope effects, and spin fluctuations in the normal state. In Sec. V, we discuss the implications of our results in the description of unconventional superconductors like the Bechgaard salts and conclude this work.

II. THE MODEL

For a linear array of $N_\perp$ chains of length L, the Hamiltonian of the quasi-1D electron gas with electron-phonon coupling is given by

$$\begin{aligned} H = H_{\rm p}^0 + H_{\rm ep} + \sum_{p,\mathbf{k},\sigma} E_p(\mathbf{k})\, c^\dagger_{p,\mathbf{k},\sigma} c_{p,\mathbf{k},\sigma} \\ + \frac{\pi v_F}{L N_\perp} \sum_{\{\mathbf{k},\sigma\}} \Big[g_1\, c^\dagger_{+,\mathbf{k}_4,\sigma_1} c^\dagger_{-,\mathbf{k}_3,\sigma_2} c_{+,\mathbf{k}_2,\sigma_2} c_{-,\mathbf{k}_1,\sigma_1} \\ + g_2\, c^\dagger_{+,\mathbf{k}_4,\sigma_1} c^\dagger_{-,\mathbf{k}_3,\sigma_2} c_{-,\mathbf{k}_2,\sigma_2} c_{+,\mathbf{k}_1,\sigma_1} \\ + \frac{1}{2} g_3 \left(c^\dagger_{+,\mathbf{k}_4,\sigma_1} c^\dagger_{+,\mathbf{k}_3,\sigma_2} c_{-,\mathbf{k}_2,\sigma_2} c_{-,\mathbf{k}_1,\sigma_1} \right. \\ \left. + \text{H.c.} \right) \Big] \delta_{\mathbf{k}_1+\mathbf{k}_2=\mathbf{k}_3+\mathbf{k}_4(\pm\mathbf{G})}, \end{aligned} \tag{1}$$

In the purely electronic part that has been made explicit, the operator $c^\dagger_{p,\mathbf{k},\sigma}$ ($c_{p,\mathbf{k},\sigma}$) creates (destroys) a right- ($p=+$) and left- ($p=-$) moving electron of wave vector $\mathbf{k}=(k,k_\perp)$ and spin σ. The free part is modeled by the anisotropic one-electron energy spectrum in two dimensions,

$$E_p(\mathbf{k}) = v_F(pk - k_F) + \epsilon(k_\perp), \tag{2}$$

where

$$\epsilon(k_\perp) = -2t_\perp \cos k_\perp - 2t'_\perp \cos 2k_\perp. \tag{3}$$

The longitudinal part has been linearized around the longitudinal Fermi wave vector given by $pk_F = \pm\pi/2$ for a dimerized chain with one electron per dimer. The longitudinal Fermi velocity is $v_F = 2t$, where t is the average nearest-neighbor hopping. Here $t_\perp$ is the nearest-neighbor hopping integral in the perpendicular direction and $t'_\perp$ is a second-nearest-neighbor hopping paramaterizing deviations to perfect nesting at $\mathbf{q}_0 = (2k_F,\pi)$, which simulates the most important effect of pressure in our model. The quasi-1D anisotropy of the spectrum is $E_F \simeq 15t_\perp$, where $E_F = v_F k_F \simeq 3000$ K is the longitudinal Fermi energy congruent with the range found in the Bechgaard salts [53–55]; E_F is taken as half the bandwidth cutoff $E_0 = 2E_F$ in the model. In the framework of the electron gas model [56,57], the interacting part of the Hamiltonian is described by the bare backward, $g_1 \equiv g_1(+k_F, -k_F; +k_F, -k_F)$, and forward, $g_2 \equiv g_2(+k_F, -k_F; -k_F, +k_F)$, scattering amplitudes between right- and left-moving electrons defined on the 1D Fermi surface. The half-filling character of the band—a consequence of a small dimerization of the chains—gives rise to Umklapp scattering of bare amplitude $g_3 \equiv g_3(\pm k_F, \pm k_F; \mp k_F, \mp k_F)$ and for which momentum conservation involves the longitudinal reciprocal lattice vector $\mathbf{G} = (4k_F,0)$. Within the electron gas model, the deviation $k \pm k_F$ of longitudinal momentum with respect to the Fermi points in the scattering amplitudes are irrelevant in the RG sense and can be neglected [56–58]. All couplings are normalized by πv_F and are initially independent of transverse momenta $k_{\perp i}$ but acquire such a dependence along the RG flow. This momentum dependence refers to the angular dependence along the Fermi surface.

Regarding the values taken by the interaction parameters throughout the present calculations, we shall take $g_1 = g_2/2 \simeq 0.32$ and $g_3 \simeq 0.025$, which follows from the phenomenological analysis of previous works that fixes their amplitude from different experiments in the weakly dimerized systems like the Bechgaard salts [31,32]. This pertains to a range of couplings generic of the interplay between SDW and SC-d orders as a function of antinesting.

The electron-phonon part of the Hamiltonian (1) follows from the modulation of the longitudinal hopping integral by acoustic phonons in the tight-binding approximation [59]. It reads

$$H_{\rm p}^0 + H_{\rm ep} = \sum_{\mathbf{q},\nu} \omega_{\mathbf{q},\nu}\left(b^\dagger_{\mathbf{q},\nu} b_{\mathbf{q},\nu} + \frac{1}{2}\right) + (LN_\perp)^{-\frac{1}{2}} \sum_{p,\sigma,\nu}\sum_{\mathbf{k},\mathbf{q}} \times g_\nu(k,q) c^\dagger_{p,\mathbf{k}+\mathbf{q},\sigma} c_{-p,\mathbf{k},\sigma}(b^\dagger_{\mathbf{q},\nu} + b_{-\mathbf{q},\nu}), \quad (4)$$

where ν is related to the different polarization of acoustic phonons. For phonons of interest propagating parallel to the chains axis, we have

$$\omega_{q,\nu} = \omega_\nu \left|\sin\frac{q}{2}\right| \quad (5)$$

for the phonon spectrum and

$$g_\nu(k,q) = i4\frac{\lambda_\nu}{\sqrt{2M\omega_\nu}} \sin\frac{q}{2}\cos\left(k+\frac{q}{2}\right) \quad (6)$$

for the electron-phonon matrix element, which depends on both electron momentum k and momentum transfer q. The coupling amplitude $\lambda_\nu = \nabla t \cdot \mathbf{e}_\nu$ is expressed in terms of the spatial variation of longitudinal hooping integral and the unit vector $\mathbf{e}_\nu$ of the lattice displacement; $\omega_\nu = 2\sqrt{\kappa_\nu/M}$ is the Debye frequency for the acoustic branch ν, and M is the mass of molecular unit. The bandwidth of acoustic branches in the molecular systems like the Bechgaard salts does not exceed $\omega_\nu \sim 100$ K [60–62]. We shall consider in the following the interval normalized phonon frequency $0 < \omega_D/t_\perp \leqslant 0.5$.

For the partition function Z, it is straightforward to proceed to the partial trace of harmonic phonon degrees of freedom and express the partition function, $Z = \int\int \mathfrak{D}\psi^*\mathfrak{D}\psi^* e^{S_0+S_I}$, as a functional integral over the fermion anticommuting fields $\psi^{(*)}$. The bare action in the Matsubara-Fourier space is given by

$$S_0[\psi^*,\psi] = \sum_{\bar{\mathbf{k}},p,\sigma} \left[G_p^0(\bar{\mathbf{k}})\right]^{-1} \psi^*_{p,\sigma}(\bar{\mathbf{k}})\psi_{p,\sigma}(\bar{\mathbf{k}}), \quad (7)$$

where $\bar{\mathbf{k}} = (\mathbf{k},\omega_n = \pm\pi T, \pm 3\pi T, \ldots)$ and

$$G_p^0(\bar{\mathbf{k}}) = [i\omega_n - E_p(\mathbf{k})]^{-1} \quad (8)$$

is the bare fermion propagator. The interacting part of the action is of the form

$$S_I[\psi^*,\psi] = -\frac{T}{LN_\perp}\pi v_F \sum_{\{\bar{\mathbf{k}},\sigma\}} \Big\{ g_1(\bar{k}_1,\bar{k}_2,\bar{k}_3,\bar{k}_4)\psi^*_{+,\sigma_4}(\bar{\mathbf{k}}_4)\psi^*_{-,\sigma_3}(\bar{\mathbf{k}}_3)\psi_{+,\sigma_2}(\bar{\mathbf{k}}_2)\psi_{-,\sigma_1}(\bar{\mathbf{k}}_1) + g_2(\bar{k}_1,\bar{k}_2,\bar{k}_3,\bar{k}_4)\psi^*_{+,\sigma_4}(\bar{\mathbf{k}}_4)\psi^*_{-,\sigma_3}(\bar{\mathbf{k}}_3) \times \psi_{-,\sigma_2}(\bar{\mathbf{k}}_2)\psi_{+,\sigma_1}(\bar{\mathbf{k}}_1) + \frac{1}{2}[g_3(\bar{k}_1,\bar{k}_2,\bar{k}_3,\bar{k}_4)\psi^*_{+,\sigma_4}(\bar{\mathbf{k}}_4)\psi^*_{+,\sigma_3}(\bar{\mathbf{k}}_3)\psi_{-,\sigma_2}(\bar{\mathbf{k}}_2)\psi_{-,\sigma_1}(\bar{\mathbf{k}}_1) + \text{c.c.}]\Big\}\delta_{\bar{\mathbf{k}}_1+\bar{\mathbf{k}}_2,\bar{\mathbf{k}}_3+\bar{\mathbf{k}}_4(\pm\bar{\mathbf{G}})} \quad (9)$$

where $\bar{k}_i \equiv (k_{\perp i},\omega_{ni})$ and $\overline{\mathbf{G}} = (4k_F,0,0)$ for Umklapp scattering. The amplitude of the bare effective backscattering is given by

$$g_1(\bar{k}_1,\bar{k}_2,\bar{k}_3,\bar{k}_4) = g_1 - \sum_\nu \frac{2}{\pi v_F\omega_\nu}\frac{g_\nu(k_F,-2k_F)g_\nu(-k_F,2k_F)}{1+(\omega_{n3}-\omega_{n1})^2/\omega_\nu^2} \equiv g_1 + \frac{g_{\rm ph}}{1+(\omega_{n3}-\omega_{n1})^2/\omega_D^2}, \quad (10)$$

where in the electron gas model scheme the interactions are defined on the 1D Fermi points with the electron-phonon matrix element evaluated at $k = \pm k_F$ and momentum transfer $q = \pm 2k_F$. Here we have defined the Debye frequency $\omega_D = \langle\omega_{2k_F,\nu}\rangle$ as the average phonon frequency over the different branches at the zone edge. We can define an attractive contribution from all acoustic branches of normalized amplitude,

$$g_{\rm ph} = -4\sum_\nu \lambda_\nu^2/(\pi v_F\kappa_\nu). \quad (11)$$

Likewise, for the amplitude of the effective forward scattering, we have

$$g_2(\bar{k}_1,\bar{k}_2,\bar{k}_3,\bar{k}_4) = g_2 - \frac{2}{\pi v_F}\sum_\nu \omega_{0,\nu}\frac{g_\nu(k_F,0)g_\nu(-k_F,0)}{\omega_{0,\nu}^2+(\omega_{n3}-\omega_{n1})^2} = g_2, \quad (12)$$

which remains unaffected by phonons at vanishing momentum transfer. Finally, for the bare Umklapp term in the presence of phonons, we have

$$g_3(\bar{k}_1,\bar{k}_2,\bar{k}_3,\bar{k}_4) = g_3 - \sum_\nu \frac{2}{\pi v_F\omega_\nu}\frac{g_\nu(k_F,2k_F)g_\nu(k_F,-2k_F)}{1+(\omega_{n3}-\omega_{n1})^2/\omega_\nu^2} \equiv g_3 + \frac{\eta|g_{\rm ph}|}{1+(\omega_{n3}-\omega_{n1})^2/\omega_D^2}, \quad (13)$$

which, in contrast to normal backscattering, gives rise to a retarded repulsive contribution, as a result of the k dependence of the electron-phonon tight binding matrix element (6). Here η is a reduction factor that takes into account the weak dimerization of the chains. For simplicity we shall take $\eta = g_3/g_1 (= \Delta_D/E_F \ll 1)$ (see also Ref. [27]).

The dependence of the above bare retarded couplings on both longitudinal k and momentum transfer q will play an important role in their RG flow at low energy.

III. RENORMALIZATION GROUP EQUATIONS

We use the finite-temperature momentum-frequency RG scheme introduced in Ref. [37]. In the partition function we proceed to the successive integration of electron states in the energy shell $\Lambda(\ell)d\ell$ at energy distance $\pm\Lambda(\ell) = \pm E_F e^{-\ell}$ from the Fermi surface, where $\ell \in [0,\infty)$. For the $k_\perp$-momentum dependence of the scattering amplitudes on each Fermi sheet, a constant energy surface in the Brillouin zone is separated into 12 patches, inside which the couplings are considered constant in the loop integration [30]. The number of patches is sufficient to take into account the nonperturbative effect of warping of the Fermi surface and the antinesting term $t'_\perp$. Regarding the frequency dependence, we have considered a finite number of $N_\omega = 14$ Matsubara frequencies ω_n ($-7 \leqslant n \leqslant 6$), within a mean-field single patch scheme for the loop frequency variable as described below. The flow equations read

$$\begin{aligned}\partial_\ell g_1(\bar{k}_1,\bar{k}_2,\bar{k}_3,\bar{k}_4) = {}& \frac{1}{2\pi}\int dk_\perp I_P(k_\perp,\bar{q}_P)[\epsilon_P\langle g_1(\bar{k}_1,\bar{k},\bar{k}_P,\bar{k}_4)g_1(\bar{k}_P,\bar{k}_2,\bar{k}_3,\bar{k})\rangle + \epsilon_{P,v}\langle g_2(\bar{k}_1,\bar{k},\bar{k}_4,\bar{k}_P)g_1(\bar{k}_P,\bar{k}_2,\bar{k}_3,\bar{k})\rangle \\ & + \epsilon_{P,v}\langle g_1(\bar{k}_1,\bar{k},\bar{k}_P,\bar{k}_4)g_2(\bar{k}_P,\bar{k}_2,\bar{k},\bar{k}_3)\rangle] + \epsilon_P\langle g_3(\bar{k}_1,\bar{k},\bar{k}_3,\bar{k}'_P)g_3(\bar{k}'_P,\bar{k}_2,\bar{k},\bar{k}_4)\rangle \\ & + \epsilon_{P,v}\langle g_3(\bar{k},\bar{k}_1,\bar{k}_3,\bar{k}'_P)g_3(\bar{k}'_P,\bar{k}_2,\bar{k},\bar{k}_4)\rangle + \epsilon_{P,v}\langle g_3(\bar{k}_1,\bar{k},\bar{k}'_P,\bar{k}_3)g_3(\bar{k}'_P,\bar{k}_2,\bar{k},\bar{k}_4)\rangle] \\ & + \frac{1}{2\pi}\int dk_\perp I_C(k_\perp,\bar{q}_C)[\epsilon_C\langle g_1(\bar{k}_1,\bar{k}_2,\bar{k},\bar{k}_C)g_2(\bar{k},\bar{k}_C,\bar{k}_4,\bar{k}_3)\rangle + \epsilon_C\langle g_2(\bar{k}_1,\bar{k}_2,\bar{k}_C,\bar{k})g_1(\bar{k},\bar{k}_C,\bar{k}_3,\bar{k}_4)\rangle], \quad (14)\end{aligned}$$

$$\begin{aligned}\partial_\ell g_2(\bar{k}_1,\bar{k}_2,\bar{k}_3,\bar{k}_4) = {}& \frac{1}{2\pi}\int dk_\perp I_P(k_\perp,\bar{q}'_P)[\,\epsilon_{P,l}\langle g_2(\bar{k}_1,\bar{k},\bar{k}_3,\bar{k}'_P)g_2(\bar{k}'_P,\bar{k}_2,\bar{k},\bar{k}_4)\rangle + \epsilon_{P,l}\langle g_3(\bar{k}_1,\bar{k},\bar{k}_P,\bar{k}_4)g_3(\bar{k}_P,\bar{k}_2,\bar{k}_3,\bar{k})\rangle] \\ & + \frac{1}{2\pi}\int dk_\perp I_C(k_\perp,\bar{q}_C)[\,\epsilon_C\langle g_1(\bar{k}_1,\bar{k}_2,\bar{k},\bar{k}_C)g_1(\bar{k},\bar{k}_C,\bar{k}_4,\bar{k}_3)\rangle + \epsilon_C\langle g_2(\bar{k}_1,\bar{k}_2,\bar{k}_C,\bar{k})g_2(\bar{k},\bar{k}_C,\bar{k}_3,\bar{k}_4)\rangle], \quad (15)\end{aligned}$$

and

$$\begin{aligned}\partial_\ell g_3(\bar{k}_1,\bar{k}_2,\bar{k}_3,\bar{k}_4) = {}& \frac{1}{2\pi}\int dk_\perp I_P(k_\perp,\bar{q}_P)2[\,\epsilon_P\langle g_1(\bar{k}_1,\bar{k},\bar{k}_3,\bar{k}'_P)g_3(\bar{k}'_P,\bar{k}_2,\bar{k},\bar{k}_4)\rangle + \epsilon_{P,v}\langle g_1(\bar{k}_1,\bar{k},\bar{k}_3,\bar{k}'_P)g_3(\bar{k}'_P,\bar{k}_2,\bar{k}_4,\bar{k})\rangle \\ & + \epsilon_{P,v}\langle g_2(\bar{k},\bar{k}_1,\bar{k}_3,\bar{k}'_P)g_3(\bar{k}'_P,\bar{k}_2,\bar{k},\bar{k}_4)\rangle] + \frac{1}{2\pi}\int dk_\perp I_P(k_\perp,\bar{q}'_P)2\epsilon_{P,l}\langle g_2((\bar{k},\bar{k}_1,\bar{k}_3,\bar{k}'_P)g_3(\bar{k}'_P,\bar{k}_4,\bar{k}_2,\bar{k})\rangle. \quad (16)\end{aligned}$$

These consist of closed-loop ($\epsilon_P = -2$), vertex corrections ($\epsilon_{P,v} = 1$), and ladder ($\epsilon_{P,l} = 1$) diagrams of the $\mathbf{q}_P$ electron-hole (Peierls) pairing, which combine with the ladder diagrams ($\epsilon_C = -1$) of the electron-electron (Cooper) pairing. Here $\bar{k}_P = \bar{k} + \bar{q}_P$, $\bar{k}'_P = \bar{k} + \bar{q}'_P$, and $\bar{k}_C = -\bar{k} + \bar{q}_C$, where $\bar{q}_{P,C} = (q_{\perp P,C},\omega_{P,C})$ corresponds to the Peierls $\bar{q}_P = \bar{k}_1 - \bar{k}_4$, $\bar{q}'_P = \bar{k}_1 - \bar{k}_3$, and Cooper $\bar{q}_C = \bar{k}_2 + \bar{k}_1$ variables.

In the above equations, each diagram singles out a discrete frequency convolution of the form $\mathcal{D}_{P,C} = \sum_{\omega_n} g_i \circ g_j \circ \mathcal{L}_{P,C}$ between the coupling products and the electronic Peierls (Cooper) loop derivative $\mathcal{L}_{P,C} = T\partial_\ell G^0_+(\bar{k}+\bar{q}_{P,C})G^0_-(\pm\bar{k})$. The exact infinite frequency summation at arbitrary T is computationally out of reach. It will be approximated, however, according to the following decoupling scheme in which the frequency summation in electronic loops is decoupled from the interactions, the latter having a frequency dependence mainly concentrated below ω_D, as shown by the phonon propagators of Eqs. (10)–(13).

We therefore use a mean-field scheme in which $\mathcal{D}_{P,C} \to \langle g_i \circ g_j\rangle \sum_{\omega_n} \mathcal{L}_{P,C}$, where $\langle\cdots\rangle = N_\omega{}^{-1}\sum_n \cdots$, stands as an average of the coupling part over a finite set of ω_n. As for the electronic part, corresponding to the ℓ derivative of the Cooper and Peierls loops, $I_{P,C} = \sum_{n=-\infty}^{+\infty}\mathcal{L}_{P,C}$, the summation over all frequencies can be computed exactly giving an explicit dependence on temperature T and external

electronic frequencies $\omega_{P,C}$. This yields

$$I_{P,C}(k_\perp,\bar{q}_{P,C}) = \sum_{\nu=\pm1} \theta[|E_0(\ell)/2+\nu A_{P,C}| - E_0(\ell)/2] \times \frac{1}{4}\left[\tanh\frac{E_0(\ell)+2\nu A_{P,C}}{4T} + \tanh\frac{E_0(\ell)}{4T}\right] \times \frac{(E_0(\ell)+\nu A_{P,C})E_0(\ell)}{(E_0(\ell)+\nu A_{P,C})^2+\omega_{P,C}^2}, \quad (17)$$

where $\omega_P = \omega_{n3} - \omega_{n1}$, and

$$A_P = -\varepsilon(k_\perp) - \varepsilon(k_\perp + q_{\perp P}) \quad (18)$$

for the Peierls channel; $\omega_C = \omega_{n1} + \omega_{n2}$ and

$$A_C = -\varepsilon(k_\perp) + \varepsilon(k_\perp + q_{\perp C}) \quad (19)$$

for the Cooper channel. Here $\theta[x]$ is the step function ($\theta[0] \equiv \frac{1}{2}$). At finite temperature, the above decoupling scheme with the number of frequencies (=14) and momentum patches (=12) retained corresponds to the solution of $(14\times12)^3 \sim 1.2\times10^6$ coupled RG flow equations governed by Eqs. (14)–(16), a number that has been reduced by various symmetries of the coupling constants with respect to frequencies and transverse momenta.

The approximation can reasonably well take into account retardation effects for a ratio $\omega_D/\pi T$ that is not too large. It represents a good compromise between exacting computing time and reproducing the results known for either the nonretarded case in quasi-1D [30–32] or the quantum corrections to the BOW ordering in a pure electron-phonon problem in one dimension [37,63].

The nature of instabilities of the electron gas and their critical temperatures, T_μ, are best studied from the susceptibilities χ_μ. For the coupled electron-phonon model under consideration, only superconducting and staggered density-wave susceptibilities present a singularity as a function of antinesting and electron-phonon interaction strength. In the static limit, these are defined by

$$\pi v_F \chi_\mu(\bar{q}_\mu^0) = \frac{1}{2\pi}\int dk_\perp \int_\ell \langle z_\mu^2(\bar{k}+\bar{q}_\mu^0)\rangle I_{P,C}(k_\perp+\bar{q}_\mu^0)d\ell, \quad (20)$$

where the vertex parts z_μ are governed by one-loop flow equations. In the density-wave channel, we shall consider

$$\partial_\ell z_{\rm SDW}(\bar{k}+\bar{q}_P^0) = \frac{1}{2\pi}\int dk'_\perp I_P(k'_\perp,\bar{q}_P^0) z_{\rm SDW}(\bar{k}'+\bar{q}_P^0) \times \langle[\epsilon_{P,l} g_3(\bar{k},\bar{k}'+\bar{q}_P^0,\bar{k}',\bar{k}+\bar{q}_P^0) + \epsilon_{P,l} g_2(\bar{k}'+\bar{q}_P^0,\bar{k},\bar{k}',\bar{k}+\bar{q}_P^0)]\rangle \quad (21)$$

and

$$\partial_\ell z_{\rm BOW}(\bar{k}+\bar{q}_P^0) = \frac{1}{2\pi}\int dk'_\perp I_P(k'_\perp,\bar{q}_P^0) z_{\rm BOW}(\bar{k}'+\bar{q}_P^0) \times \langle[\epsilon_P g_1(\bar{k}'+\bar{q}_P^0,\bar{k},\bar{k}',\bar{k}+\bar{q}_P^0) + \epsilon_{P,l} g_2(\bar{k}'+\bar{q}_P^0,\bar{k},\bar{k}',\bar{k}+\bar{q}_P^0) - \epsilon_P g_3(\bar{k}',\bar{k}+\bar{q}_P^0,\bar{k}'+\bar{q}_P^0,\bar{k}) - \epsilon_{P,l} g_3(\bar{k},\bar{k}'+\bar{q}_P^0,\bar{k}',\bar{k}+\bar{q}_P^0)]\rangle \quad (22)$$

for the static μ = SDW and BOW susceptibilities, respectively, at $\bar{q}_P^0 = (\pi,0)$. In the superconducting channel, we shall examine

$$\partial_\ell z_\mu(-\bar{k}+\bar{q}_C^0) = \frac{1}{2\pi}\int dk'_\perp I_C(k'_\perp,\bar{q}_C^0) z_\mu(-\bar{k}'+\bar{q}_C^0) \times \Delta_\mu(k_\perp)\langle\epsilon_C[g_1(-\bar{k}'+\bar{q}_C^0,\bar{k}',-\bar{k}+\bar{q}_C^0,\bar{k}) + g_2(-\bar{k}'+\bar{q}_C^0,\bar{k}',\bar{k},-\bar{k}+\bar{q}_C^0)]\rangle, \quad (23)$$

for the static SC susceptibility at $\bar{q}_C^0 = 0$, where $\Delta_\mu(k_\perp)$ is the form factor for the SC order parameter. For SC-d and triplet-f wave (SC-f) correlations, we have $\Delta_{{\rm SC}-d}(k_\perp) = \sqrt{2}\cos k_\perp$ and $\Delta_{{\rm SC}-f}(k_\perp) = ({\rm sgn}\, k)\sqrt{2}\cos k_\perp$, whereas for conventional singlet pairing (SC-s) we have $\Delta_{{\rm SC}-s}(k_\perp) = 1$.

Before embarking on the solution of the above equations, it is instructive at this stage to examine their basic features as a function of the different energy scales of the model. At high temperature where $T \gg \omega_D$ and the phonons are classical, the contribution of the Ph-M interaction to all open diagrams—ladder and vertex corrections—becomes strongly dampened for all $\Lambda(\ell)$, as a result of retardation that reduces the summations over intermediate frequency transfer in such diagrams. In this temperature range, the Ph-M part contributes more appreciably to the closed-loop diagram of the Peierls channel which does not have an intermediate sum over transfer frequencies, and this is on equal footing with the direct Coulomb part in Eqs. (14)–(16). On the other hand, when entering the low-temperature domain at $T < \omega_D$, retardation effects are reduced which progressively strengthen the contribution of the electron-phonon interaction to open diagrams. This increases mixing or interference between all diagrams of the Peierls and Cooper scattering channels.

For the range of parameters considered in the model, the temperature scale T_μ of instabilities of the electron gas that are considered below all fall in the temperature range $T_\mu \ll t_\perp$. This is where the transverse electron motion and the warping of the Fermi surface are coherent, making the electron gas effectively two-dimensional, albeit strongly anisotropic in this temperature domain. This is known to affect the interference in a particular way depending on the energy distance $\Lambda(\ell)$ from the Fermi surface in the RG flow. At high energy, when $\Lambda(\ell) \gg t_\perp$, the flow essentially coincides with the 1D limit where the interference is maximum, although subjected to the above conditions between T and ω_D. When $\Lambda(\ell) \ll t_\perp$, the interference between the Peierls and Cooper channels is affected by the coherent warping of the Fermi surface and ultimately nesting alterations at $\Lambda(\ell) < t'_\perp$. Both generate a momentum dependence of the coupling constants (14)–(16) which reflects in the end the nature of the electron gas instability at T_μ.

IV. RESULTS

A. Instabilities for weak phonon-mediated interaction

The integration of the RG equations up to $\ell \to \infty$ for the couplings (14)–(16) and pair vertices (21)–(23) leads to the temperature dependence of the selected susceptibilities as a function of antinesting, $t'_\perp/t_\perp$, phonon frequency, $\omega_D/t_\perp$, both

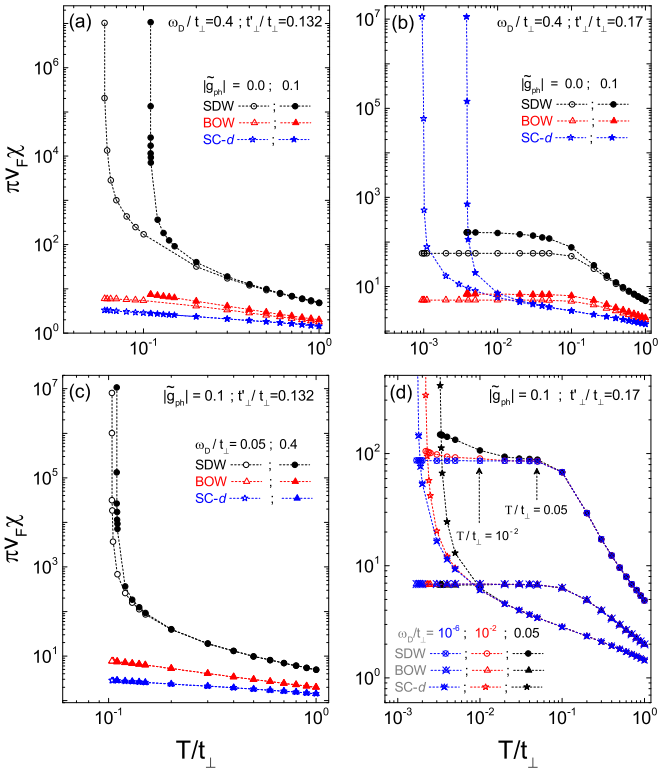

FIG. 1. (Color online) Typical temperature variations of the SDW, BOW, and SC-d-wave susceptibilities at $\omega_D/t_\perp = 0.4$ for (a) weak and (b) intermediate antinesting $t'_\perp$ at zero (open symbols) and a nonzero (solid symbols, $|\tilde{g}_{\rm ph}| = 0.1$) phonon-mediated interaction. The comparison of susceptibilities for the same $|\tilde{g}_{\rm ph}|$ for weak (c) and intermediate (d) antinesting values at lower phonon frequencies.

normalized by the interchain hopping $t_\perp$; as for the weak Ph-M interaction, it is parameterized by the ratio

$$|\tilde{g}_{\rm ph}| \equiv |g_{\rm ph}|/g_1, \tag{24}$$

here normalized by the strength of nonretarded repulsive interaction g_1. The main features the influence of weak Ph-M coupling has on the temperature dependence of relevant susceptibilities are summarized in Fig. 1 at small and intermediate antinesting parameter $t'_\perp$, and different ω_D. In Fig. 1(a), $t'_\perp$ is taken sufficiently small so nesting promotes a singularity in $\chi_{\rm SDW}$, indicating an instability against the onset of SDW order at $T_{\rm SDW}$. As for the correlations in the BOW and SC-d channels, the related susceptibilities are nonsingular and remain small. According to Fig. 1(a), the presence of an even small $|\tilde{g}_{\rm ph}|$ at sizable ω_D is sufficient to cause a noticeable increase of $T_{\rm SDW}$ compared to the purely electronic limit.

At the outset, the strengthening of SDW instability takes its origin in the k and q momentum dependence of Ph-M interaction in Eqs. (10)–(13) at $\ell = 0$, resulting in a reduction of the backscattering and an increase of the Umklapp term. As discussed in more detail in Sec. IV C 1, when Ph-M terms are small compared to unretarded interactions, both concur to an increase of antiferromagnetic spin exchange between itinerant electrons of opposite spins and located on separated sheets of the Fermi surface near $\pm k_F$. The above effects on scattering amplitudes are magnified by the RG flow, mainly due to nesting in one-loop ladder and vertex corrections. Moreover, the reinforcement of SDW becomes the most efficient in the temperature range $T < \omega_D$ due to the reduction of retardation. This is where the Ph-M part acts progressively as nonretarded contributions in all open diagrams such as the ladder and vertex corrections of (14)–(16) and (21), namely, those mainly involved in the exchange mechanism. The influence of Ph-M coupling on SDW correlations will then naturally depend on the value of phonon frequency ω_D. Figure 1(c) shows indeed that lowering ω_D reduces the enhancement of $T_{\rm SDW}$ at low antinesting, an indication of a positive isotope effect on SDW (see Sec. IV C 1).

At large-enough $t'_\perp$, nesting turns out to be sufficiently poor to prevent the occurrence of SDW. The instability of the metallic state no longer takes place in the density-wave channel but rather shows up by interference in the Cooper channel with the onset of SC-d order at T_c. As shown in Fig. 1(b), the presence of a small Ph-M coupling at the same ω_D gives rise to a substantial increase of the critical temperature T_c compared to the purely electronic case. The SC-d strengthening is the mere consequence of the boost of SDW spin fluctuations responsible for the Cooper pairing in the metallic state. This is shown in Fig. 1(b) where at nonzero $|\tilde{g}_{\rm ph}|$ a more pronounced, though nonsingular, enhancement of $\chi_{\rm SDW}$ is found above T_c. This feature signals that the reinforcement of spin fluctuations persists relatively deep in the normal state.

In Fig. 1(d) the effect of ω_D on both T_c and normal state spin fluctuations is singled out. The growth of T_c with ω_D is correlated with the increase of spin correlations above T_c. In this part of the figure, we note that the onset of spin fluctuation reinforcement takes place at $T < \omega_D$, where $\chi_{\rm SDW}$ clearly separates from the static $\omega_D \to 0$ limit; it signals the growth of ladder and vertex corrections following a reduction of retardation. The enhancement of spin fluctuations in the normal phase will be analyzed in Sec. IV D, where it is found to follow a Curie-Weiss temperature dependence, which is comparatively more pronounced than the one occurring in the purely electronic limit [31,32].

Concerning BOW correlations, Fig. 1 shows that for weak $|\tilde{g}_{\rm ph}|$, these remain weakly enhanced. However, as will be shown next, the situation qualitatively changes when $|\tilde{g}_{\rm ph}|$, though still small, reaches some critical value.

B. Phase diagrams

1. *Spin-density-wave versus d-wave superconductivity*

We now consider the sequence of instabilities of the metallic state as a function of $t'_\perp$ in order to construct the phase diagrams at weak Ph-M couplings. This is shown in Fig. 2(a). At small $|\tilde{g}_{\rm ph}|$ and for a sizable ω_D, the system remains unstable to the formation of a SDW state with a $T_{\rm SDW}$ that displays the characteristic monotonic decrease with increasing $t'_\perp$ [26,29–32,64,65]. At the approach of a well-defined antinesting threshold $t'^*_\perp$, however, $T_{\rm SDW}$ undergoes a critical drop that terminates at $t'^*_\perp$, where SC-d begins at its peak value denoted by T^*_c. Above, T_c shows a continuous decrease with $t'_\perp$ that correlates with the reduction of SDW fluctuations as the source of Cooper pairing.

As stressed above, Fig. 2(a) confirms that the Ph-M coupling, albeit small, reinforces both $T_{\rm SDW}$ and T_c for all

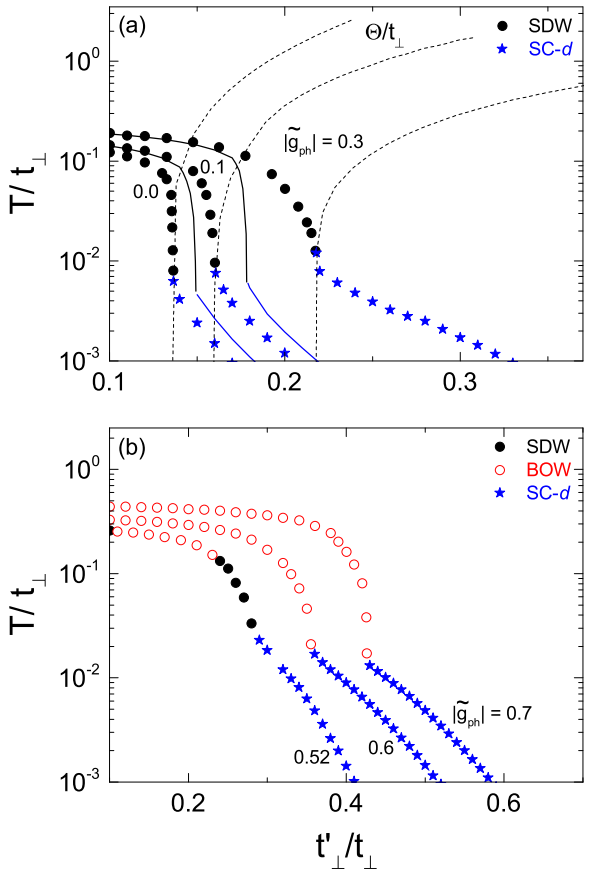

FIG. 2. (Color online) Phase diagrams of the repulsive quasi-1D electron gas model as a function of the antinesting parameter $t'_\perp$ and $|\tilde{g}_{\rm ph}|$ for (a) the SDW–SC-d and (b) BOW–SC-d sequences of instabilities at $\omega_D/t_\perp = 0.4$. In (a), the continuous lines correspond to the instability lines in the adiabatic $\omega_D \to 0$ limit and the dashed lines show the variation of the Curie-Weiss scale Θ of $\chi_{\rm SDW}$ [Eq. (26)] as a function of $t'_\perp$ in the superconducting region.

$t'_\perp$, including the critical value $t'^*_\perp$ at which superconductivity emerges. We also note from Fig. 2(a) that this reinforcement reduces the sharpness of its critical drop at the approach of $t'^*_\perp$, an effect that carries over in the superconducting sector where the reduction of T_c with $t'_\perp$ turns to be less rapid.

Also shown in the figure are the instability lines in the static $\omega_D \to 0$ limit [continuous lines of Fig. 2(a)]. Retardation effects are found to be very important at the approach of the critical value $t'^*_\perp|_{\omega_D\to 0}$ and beyond, an indication that the isotope effect is clearly nonuniform as a function of $t'_\perp$ (see Sec. IV C 1). It is also worth noticing from the figure that in the presence of dominant nonretarded repulsive interactions, the influence of Ph-M terms on both SDW and SC-d instabilities remains finite in the static limit. This contrasts with the situation when only Ph-M interactions are present, and where $T_c \to 0$ as $\omega_D \to 0$ for s-wave SC [37].

2. Bond-order wave versus superconductivity

By increasing further the strength of Ph-M coupling for the same ω_D, Fig. 2(b) shows that the SDW–SC-d sequence of instabilities as a function of $t'_\perp$ is maintained only up to a critical $|\tilde{g}^c_{\rm ph}|$ ($\approx$0.52 for the parameters used), above which SDW turns out to be no longer stable and replaced by the onset of a nonmagnetic BOW state at $T_{\rm BOW}$. The typical variations of relevant susceptibilities in the BOW sector of the phase diagram are given in Fig. 3(a). The BOW instability that takes place from the metallic state corresponds to the onset of a Peierls, though correlated, lattice distorted state [63,66].

A remarkable feature of the phase diagrams of Fig. 2(b) is that above $|\tilde{g}^c_{\rm ph}|$ and at ω_D that is not too small, the BOW instability continues to be followed by SC-d superconductivity at $t'_\perp \geqslant t'^*_\perp$. In these conditions, however, T_c becomes a decreasing function of $|\tilde{g}_{\rm ph}|$. This is depicted in Fig. 4, where it behaves so after having reached its maximum at the boundary $|\tilde{g}^c_{\rm ph}|$ where SDW and BOW are found to be essentially degenerate and at their maximum strength. It is worth noticing that at the boundary, T_c has increased by a factor 4 or so compared to the purely electronic case. Despite the presence of a Peierls lattice distorted state, the essential role played by spin fluctuations in the emergence of SC-d at $t'_\perp \geqslant t'^*_\perp$ remains. This is confirmed in Fig. 3(b), where $\chi_{\rm SDW} > \chi_{\rm BOW}$ over a large temperature interval at the approach of T_c in the normal state. In this sector we find no sign of increase for the s-wave superconducting correlations, as shown by the temperature profile of $\chi_{{\rm SC}-s}$ that displays no enhancement in Fig. 3(b). It is only when $|\tilde{g}_{\rm ph}| \gtrsim 1$ that SC-d becomes in turn unstable and BOW ordering gives rise to s-wave superconductivity under nesting alteration. The latter case has been analyzed in detail by the same technique in Ref. [37].

Another surprising feature of the phase diagram in $|\tilde{g}_{\rm ph}| > |\tilde{g}^c_{\rm ph}|$ is found at low phonon frequency. Figure 5 shows that in the small-ω_D range, the BOW ordering at $t'_\perp \geqslant t'^*_\perp$ is followed by a triplet SC-f instability instead of a SC-d one. Since small phonon frequency increases retardation, it reinforces most exclusively closed-loop diagrams in the RG flow, related to density or charge fluctuations. Bond charge correlations are then increased with respect to their spin counterpart, and for dominant repulsive interactions, this leads to SC-f-type superconductivity. The triplet-singlet competition is in a way reminiscent of the one found when a weak, repulsive (nonretarded) interchain interaction is added to the purely repulsive quasi-1D electron gas model [30]. The latter coupling is also known to boost exclusively charge fluctuations [67], similar to the way electron-phonon interaction does for closed loops when strong retardation is present; the same interchain coupling is also known to promote a SDW-to-BOW crossover in the density-wave instabilities at low antinesting [30]. Cranking up ω_D results in the progressive enhancement of open diagrams which are responsible for spin fluctuations and d-wave superconductivity. Although, from Fig. 5, the BOW ordering is weakly affected, a SC-$f \to$ SC-d crossover is indeed found to occur at small $\omega_D/t_\perp$ ($\sim$0.1 for the parameters used).

C. Isotope effects

1. Spin-density-wave and d-wave superconductivity

In the preceding paragraphs we mentioned on several occasions the positive influence of raising ω_D on the strength of SDW and SC-d instabilities. This result, obtained by varying the molecular mass M at fixed elastic constant κ [$g_{\rm ph}$, which remained constant according to Eq. (11)], corresponds

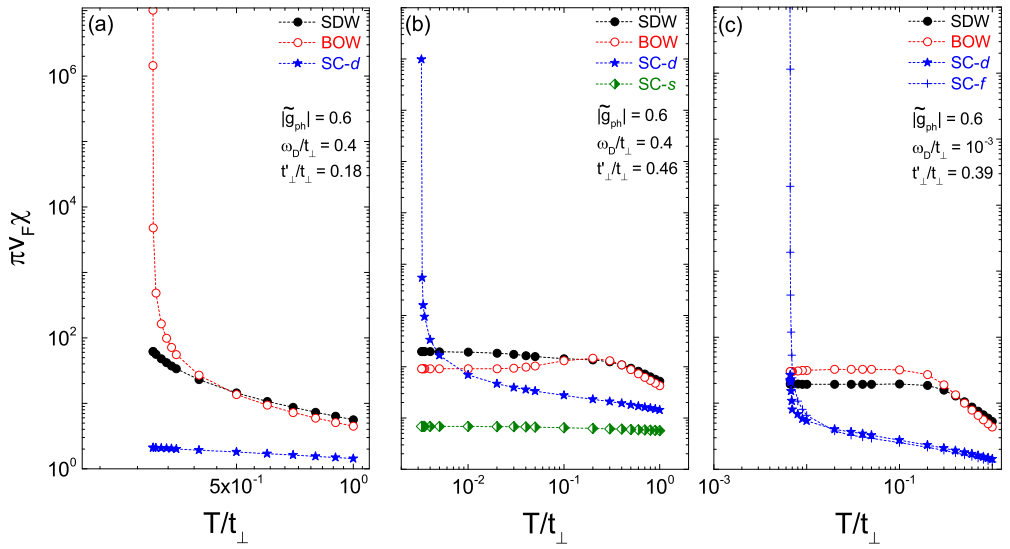

FIG. 3. (Color online) Temperature variation of the SDW, BOW, and SC-d susceptibilities for $|\tilde{g}_{\rm ph}|$ above the threshold $|\tilde{g}^{\rm c}_{\rm ph}|$ for the occurrence of BOW instability at (a) $t'_\perp < t'^*_\perp$ and in the superconducting sector at $t'_\perp > t'^*_\perp$ for the (b) SC-d ($\omega_D/t_\perp = 0.4$) and (c) triplet SC-f ($\omega_D/t_\perp = 10^{-3}$) instabilities.

to a positive isotopic effect. As touched on previously, the mechanism of reinforcement of SDW correlation can be understood as a modification of the effective antiferromagnetic exchange mechanism, itself affected by retardation. Actually, for itinerant electrons, the total scattering amplitudes g_2 and g_3 of the action S_I in (9) contribute at T an exchange term of the form

$$S_I^{\rm ex} = \pi v_F \frac{T}{LN_\perp} \sum_{\{\bar{\mathbf{k}}\},\bar{\mathbf{q}}_P} \frac{1}{2}(g_2 + g_3) \circ \vec{S}_{\bar{\mathbf{k}}_1,\bar{\mathbf{q}}_P} \cdot \vec{S}_{\bar{\mathbf{k}}_2,-\bar{\mathbf{q}}_P}, \quad (25)$$

where $\vec{S}_{\bar{\mathbf{k}},\bar{\mathbf{q}}_P} = \frac{1}{2}\psi^*_{+,\alpha}(\bar{\mathbf{k}}+\bar{\mathbf{q}}_P)\vec{\sigma}^{\alpha\beta}\psi_{-,\beta}(\bar{\mathbf{k}}) + \text{c.c.}$ is the Fourier-Matsubara component of the SDW spin density. Thus in weak coupling, the combination $\frac{1}{2}(g_2+g_3)$ corresponds to a momentum- and frequency-dependent antiferromagnetic exchange interaction generated by the scattering of oppositely moving carriers at $\pm k_F$ with antiparallel spins. It is the same exchange term that governs the enhancement of the vertex part $z_{\rm SDW}$ for the SDW susceptibility [see Eq. (21)]. Its growth with decreasing $\Lambda(\ell)$ results from the multiple exchange scattering of virtual $\mathbf{q}_P$ electron-hole pairs carried by ladder and vertex corrections in the flow equations (15) and (16). As to the backscattering term, g_1, its role is indirect since in the repulsive sector, g_1 tends to align spins of $\pm k_F$ carriers. This dampens the amplitude of both g_2 and g_3 and then SDW correlations. Therefore, by lowering $\Lambda(\ell)$, the combined influence of a g_1 reduction and a g_3 increase by Ph-M interactions in (10) and (13) will boost g_2 and, in turn, g_3 and antiferromagnetic exchange. As mentioned earlier, however, this additional and positive input of Ph-M interaction reaches

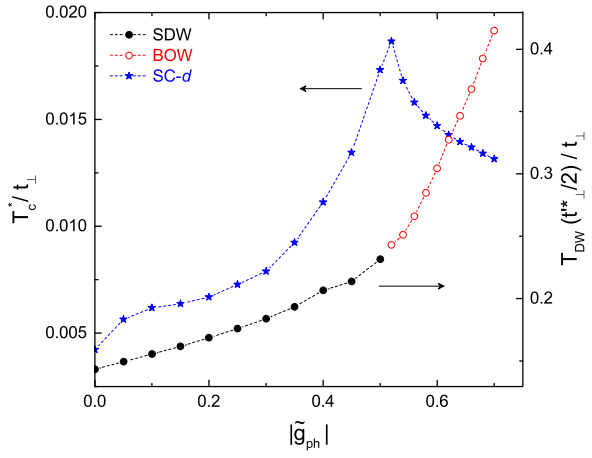

FIG. 4. (Color online) SDW-BOW critical temperatures at $t'_\perp = t'^*_\perp/2$ below the threshold antinesting (right) and the maximum SC-d critical temperature (left) [$T_c^* = T_c(t'^*_\perp)$] versus the normalized strength of phonon-mediated interaction $|\tilde{g}_{\rm ph}|$ at $\omega_D/t_\perp = 0.4$.

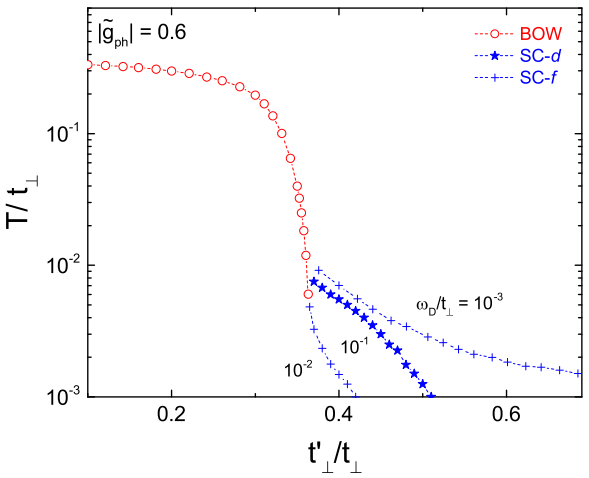

FIG. 5. (Color online) Phase diagram above the threshold $|\tilde{g}^{\rm c}_{\rm ph}|$ for the BOW-to-SC sequence of instabilities as a function of antinesting. The figure shows the crossover between triplet f-wave and singlet d-wave superconductivity in the small phonon frequency region.

its maximum impact in the temperature domain $T < \omega_D$, namely where retardation effects on virtual electron-hole pair scattering processes become small, hence the isotope effect on SDW.

The increase of $T_{\rm SDW}$ with ω_D is illustrated in Fig. 6(a) for $|\tilde{g}_{\rm ph}| = 0.1$ and different values of $t'_\perp$ in the SDW part of the phase diagram. At relatively small $t'_\perp$ that is, well into the SDW sector, $T_{\rm SDW}$ undergoes a monotonic but weak increase over all the frequency range of phonons, a consequence of ladder and vertex corrections to the antiferromagnetic exchange that grow in importance by increasing ω_D. It is worth noticing that in the adiabatic limit, $T_{\rm SDW}|_{\omega_D \to 0}$ is found to be slightly larger than the $T_{\rm SDW}|_{g_{\rm ph}=0}$ obtained in the absence of Ph-M interaction [see Fig. 2(a)]. This indicates that static phonons still have a positive influence on the exchange interaction (25) and the strength of SDW correlations. This adiabatic effect finds a certain echo in the strong coupling—Hubbard interaction—case where dynamical mean-field theory calculations do predict an enhancement of antiferromagnetic exchange between localized spins by zero-frequency phonons [45]. Here the static enhancement essentially results from the mixing of Ph-M interaction to the nonretarded Coulomb terms g_i in the RG flow; the enhancement vanishes by taking $g_i \to 0$ in Eqs. (10), (12), and (13), a result found in the limit of pure electron-phonon coupling [37].

When $t'_\perp$ increases and approaches the critical domain where the drop in $T_{\rm SDW}$ becomes, according to Fig. 2(a), essentially vertical, the isotope effect becomes huge as traced in Fig. 6(a). Close to $t'^*_\perp$, the reinforcement of SDW correlations by an even small increase in ω_D gives rise a large increase of $T_{\rm SDW}$. This is not the consequence of nesting improvement but rather the result of stronger nesting deviations needed to counteract the reinforcement of SDW instability by Ph-M interactions. For $t'_\perp$ slightly above $t'^*_\perp$, Fig. 6(a) features the interesting possibility of a SC-d-to-SDW transition as a function of ω_D.

The positive isotope effect carries over into the SC-d side of the phase diagram where T_c is found to increase with ω_D at different $t'_\perp$, as shown in Fig. 6(b). This is directly associated with the ω_D-dependent reinforcement of spin correlations in the normal state as already pointed out in Fig. 1(d), which strengthens the pairing interaction in the SC-d channel. Although the isotope effect is slightly larger in amplitude near the critical $t'^*_\perp$, it remains of comparable size at an arbitrary value of antinesting with a power law $T_c \sim \omega_D^\alpha$ that takes place at an intermediate frequency with an exponent $\alpha \simeq 0.24 (\equiv d \ln T_c / d \ln \omega_D)$, a value virtually independent of $t'_\perp$ [see Fig. 6(b)] and $|\tilde{g}_{\rm ph}|$, as shown in the insert of Fig. 6(b). At high phonon frequency where the ratio ω_D / T_c becomes very large, retardation effects become negligible and T_c tends to level off with frequency. This saturation probably reflects the limitation of using a finite number of Matsubara frequencies in the mean-field approximation of the loop convolution over frequency.

2. *Bond-order wave versus superconductivity*

In the BOW regime above $|\tilde{g}^c_{\rm ph}|$, the isotope effect on $T_{\rm BOW}$ has the opposite sign. At low $t'_\perp$, for instance, Fig. 7(a) shows that $T_{\rm BOW}$ decreases monotonically with ω_D and the reduction becomes increasingly large with $t'_\perp$ which also softens the lattice distortion through nesting alteration. A reduction of $T_{\rm BOW}$ with ω_D is a consequence of the growth of nonadiabaticity of the phonon field, a well-known factor to be at play in the reduction of the Peierls distortion gap in purely electron-phonon models in one dimension [63,66,68]. From a diagrammatic point of view, nonadiabaticity is a quantum effect again tied to the unlocking of Ph-M interaction to open diagrams and thus to quantum interference between electron-hole and Cooper pairing at the one-loop level. In contrast to the SC–d/SDW mixing, however, the interference is, in the present, case destructive: Cooper and Peierls diagrammatic contributions have opposite sign and this reduce the temperature scale of BOW ordering [66]. The onset of a quantum to classical crossover for the BOW state is perceptible at $\omega_D / 2T^0_{\rm BOW}|_{\omega_D \to 0} \sim 1$, as is found to occur in the pure electron-phonon limit [37,63].

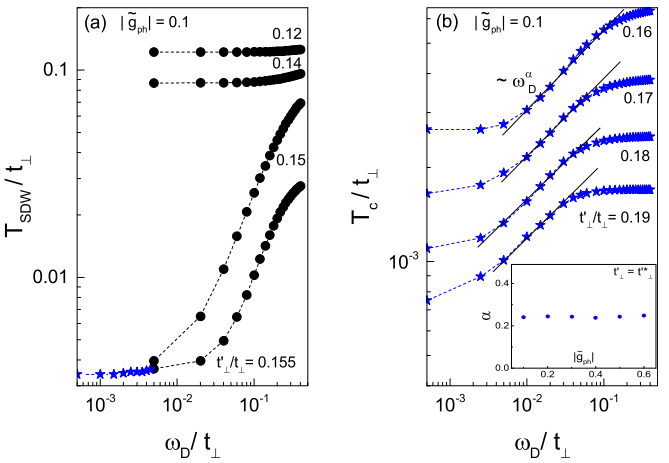

FIG. 6. (Color online) Isotope effect at $|\tilde{g}_{\rm ph}| = 0.1$ for (a) $T_{\rm SDW}$ at different antinesting $t'_\perp < t'^*_\perp$ and (b) T_c of the SC-d channel for different $t'_\perp > t'^*_\perp$. Insert: Variation of the isotope exponent as a function of phonon-mediated coupling amplitude at $t'^*_\perp$.

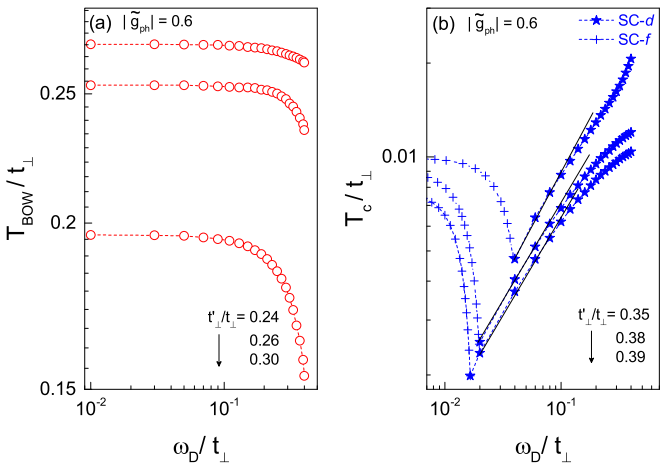

FIG. 7. (Color online) Isotope effect at $|\tilde{g}_{\rm ph}| > |\tilde{g}^c_{\rm ph}|$ for (a) $T_{\rm BOW}$ at different antinesting $t'_\perp < t'^*_\perp$ and on (b) T_c in the SC-f and SC-d channels for different $t'_\perp > t'^*_\perp$. The straight lines correspond to the power-law dependence $T_c \sim \omega_D^\alpha$, where $\alpha \simeq 0.25$.

Above $t_\perp'^*$, but for small ω_D, we still observe an inverse isotope effect for the T_c of triplet, SC-f superconductivity, as shown in Fig. 7(b). This confirms the role of BOW fluctuations in the existence of SC-f ordering at repulsive coupling. This is further supported when ω_D increases and crosses the critical value at which SC-d reappears in Fig. 5. Then the isotope effect becomes once again positive as a consequence of the growth of antiferromagnetic exchange and spin fluctuations that govern the d-wave Cooper pairing. In the SC-d regime, one can extract at intermediate frequencies a power-law dependence $T_c \sim \omega_D^\alpha$ for the isotope effect with a value of $\alpha \simeq 0.25$ similar to the one found below $|\tilde{g}_{\rm ph}^c|$ [Fig. 6(b)].

D. Normal state

Now that the positive influence of electron-phonon interactions on the temperature scales for ordering has been examined, one can turn our attention on the influence of a weak Ph-M interaction on spin correlations of the normal phase above T_c. This is done for the SDW–SC-d sequence of instabilities. In Fig. 8(a), we show the temperature dependence of the inverse SDW susceptibility at small $|\tilde{g}_{\rm ph}|$ and various strengths of antinesting. At sufficiently high $t_\perp' > t_\perp'^*$, $\chi_{\rm SDW}^{-1}$ decays essentially linearly from the high-temperature region and extrapolates towards a critical point at a finite $T_{\rm SDW}$. However, as the temperature is lowered at $T < t_\perp'$, nesting deviations becomes coherent and the susceptibility undergoes a change of regime and ceases to be critical. Nevertheless, according to Fig. 8(a), $\chi_{\rm SDW}^{-1}$ keeps decreasing and extrapolates to a nonzero intercept at $T = 0$ and a finite slope at the end point T_c.

This nonsingular growth of spin correlations in the metallic state, which persist down to T_c, can be well described by a Curie-Weiss form (continuous lines in Fig. 8),

$$\chi_{\rm SDW} = \frac{C}{T + \Theta}, \tag{26}$$

extending up to the temperature $T_{\rm CW}$ for the onset of the Curie-Weiss regime, which is about 10 times T_c in temperature

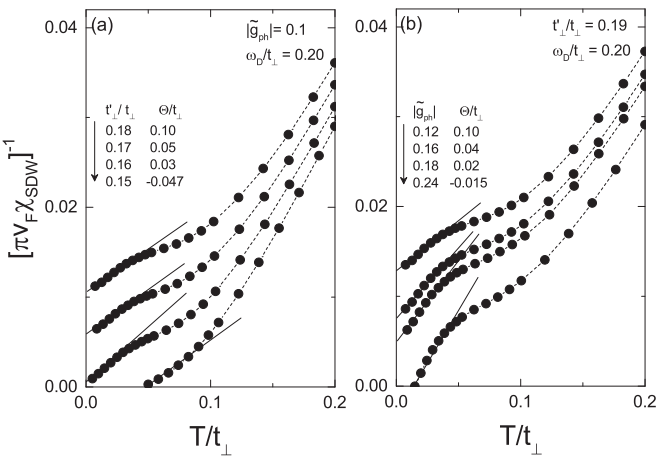

FIG. 8. The temperature dependence of the normal phase inverse SDW susceptibility at different antinesting (a) and electron-phonon interaction strengths (b). The straight lines correspond to the Curie-Weiss fit [Eq. (26)].

at the frequency used in the figure $\{T_{\rm CW}$ decreases when ω_D is lowered [see Fig. 1(d)]$\}$. Here the Curie-Weiss scale Θ stands as a characteristic energy for SDW fluctuations, which is defined as positive when $t_\perp' > t_\perp'^*$. The Curie-Weiss behavior has been already found in the purely electronic case [31,32]. It results from the positive feedback of SC-d pairing on SDW correlations, a consequence of constructive interference between these channels of correlations. The presence of Ph-M interactions clearly reinforces this behavior. As shown in Fig. 8(b), cranking up $|\tilde{g}_{\rm ph}|$ leads to the decrease of the Curie-Weiss scale Θ and an increase of the constant C. This is consistent with an increase of the SDW correlation length $\xi \sim (T + \Theta)^{-1/2}$, in tune with the increase of T_c discussed above. The softening of Θ in Fig. 8 carries on until $t_\perp'$ reaches $t_\perp'^*$ where $\Theta \to 0$. There the system would then become quantum critical with $\chi_{\rm SDW} \sim 1/T$ and $T_{\rm SDW} \to 0$, if not for the presence of superconductivity at a finite T_c that prevents the SDW quantum critical point from being reached. Below $t_\perp'^*$, $\Theta < 0$ and the system enters the SDW sector with a finite $T_{\rm SDW}(\equiv -\Theta) > T_c$.

At the approach of $t_\perp'^*$, Θ is well fitted by the quantum scaling form

$$\Theta \approx A(t_\perp' - t_\perp'^*)^\eta, \tag{27}$$

with an exponent $\eta \simeq 1$, consistently with the product $\eta = \nu z$ of the correlation length ($\nu = 1/2$) and the dynamical ($z = 2$) exponents for SDW at the one-loop level. The linear profile of Θ near $t_\perp'^*$ is illustrated in Fig. 2(a). From the Fig. 2(a) and Fig. 8(b), the coefficient A decreases relatively quickly with $|\tilde{g}_{\rm ph}|$.

V. DISCUSSION AND CONCLUSION

In this work we used a weak-coupling RG approach to examine the influence of the tight-binding electron-phonon interaction on the interplay between magnetism and superconductivity in quasi-one-dimensional correlated electron systems. When the phonon-mediated interaction remains weak and subordinate to the direct Coulomb terms of the electron gas, the RG flow of scattering amplitudes is found to be distorted for particular longitudinal electron momentum and momentum transfers. This reinforces the antiferromagnetic exchange mechanism between itinerant spins and yields an increase of the temperature scale of SDW ordering. By introducing enough nesting deviations into the electron kinetics, SDW ordering is inhibited, but magnetic reinforcement by the electron-phonon interaction persists and shifts by interference in the superconducting channel. d-Wave Cooper pairing and T_c then become enhanced compared to the purely electronic situation. These properties were found to be affected by retardation effects linked to the exchange of low-energy acoustic phonons that modulate the strength of virtual electron-hole scattering entering into the antiferromagnetic exchange term of the electron gas. This gives rise to a positive isotope effect on the SDW ordering temperature, which carries over beyond the critical antinesting $t_\perp'^*$ where d-wave superconductivity is found.

Our results also revealed that such an increase for T_c is preceded by the strengthening of spin fluctuations in the normal phase. This is manifest in a more pronounced Curie-

Weiss SDW susceptibility compared to the purely electronic situation, a consequence of self-consistency between d-wave Cooper pairing and spin fluctuations, a positive interference effect whose amplitude scales with T_c.

We have also established the range of electron-phonon interaction beyond which SDW ordering is no longer stable against the BOW or Peierls distorted state. In these conditions, the Peierls ordering was found to be followed above critical antinesting by either d-wave or, amazingly, triplet f-wave superconductivity depending if the retardation effects are weak or strong, respectively. The isotope effect which is negative in the triplet SC-f sector and positive in SC-d reflects the origin of the pairing interaction in both situations, namely BOW fluctuations in the former case and SDW ones in the latter.

The relevance of the above results for concrete materials showing the emergence of superconductivity on the verge of antiferromagnetism is of interest. In Bechgaard salts, for instance, superconductivity manifests itself where SDW state ends under pressure. Their normal state is characterized by important spin fluctuations over a large temperature interval above T_c whose amplitude scales with the one of spin correlations under pressure, as made abundantly clear by NMR experiments [22,25,69,70].

Our findings show that intrachain repulsive interactions are dominant in these materials. While repulsive interactions are known to be able to generate on their own the sequence of SDW-SC-d instabilities as a function $t'_\perp$ in the quasi-1D electron gas model [29–32], the present results show, however, that the addition of a relatively small tight-binding electron-phonon interaction, which would be compatible with diffuse x-ray scattering experiments [34,35], are far from being an obstacle for superconductivity. When subordinate to the purely electronic repulsion, the phonon-mediated interaction can indeed play a very active part in assisting antiferromagnetism in the emergence of d-wave superconductivity with a stronger T_c.

Although the typical range of values taken by the electron-phonon matrix element has not been determined with great accuracy in materials like the Bechgaard salts (see, for example, Ref. [71]), the results of the present paper suggest that it should be small in amplitude compared to direct interactions. This is supported by the stability of the SDW state against the Peierls distortion, which, from the above results, is found to be assured only within a finite interval of weak phonon-mediated interaction at essentially arbitrary retardation. Therefore the absence of the Peierls phenomena in the Bechgaard salts may be viewed as a mere consequence of the weakness of the electron-phonon coupling constant in these materials. This view would be consistent with previous estimations made from optics [71] and also from the fact that the only few materials showing a lattice distorted phase belong to the more correlated isostructural compounds of the $(TMTTF)_2X$ series, the so-called Fabre salts. A compound like $(TMTTF)_2PF_6$, for instance, is well known to undergo a spin-Peierls transition within a strongly correlated Mott state [34,35,72]. Less than 10 kbars of pressure is sufficient to weaken the coupling of phonons to electrons and transform this state into one with antiferromagnetic Néel order [73,74]; 30 kbars separate the latter from the sequence of SDW-SC instabilities found in the prototype compound $(TMTSF)_2PF_6$ of the Bechgaard salts [75–77], in line with a coupling to phonons that remains in the background of direct Coulomb terms.

As to the possible experiments able to disentangle the part played by phonon-mediated interaction on the SDW-SC sequence of instabilities seen in molecular materials like the Bechgaard salts, isotope effect measurements would be certainly of interest, especially near the quantum critical point where the present results show that it becomes huge at the approach of $t'^*_\perp$ on the SDW side of the phase diagram. While the isotope effect in molecular materials proves to be difficult to realize in practice due to the complications of controlling all other parameters following a change in the mass M of molecular units (volume of the unit cell, disorder, etc.), the ^{13}C enrichment of the TMTSF molecular units stands probably as the best way to limit these side effects and to test some of the results obtained here. According to Fig. 2(a), for instance, a finite reduction in ω_D would induce a decrease in the critical $t'^*_\perp$ at which superconductivity occurs. Practically, one should therefore expect a downward shift of the critical pressure for the emergence of superconductivity and a decrease in the maximum T^*_c at that point and beyond on the pressure axis.

Another possible signature of the reinforcement of antiferromagnetism by electron-phonon interaction in the Bechgaard salts may be found in its influence on the Curie-Weiss behavior of SDW susceptibility which governs the enhancement of the NMR spin-lattice relaxation rate observed down to T_c [22,25,69,78,79]. While the quasi-1D electron gas model with purely electronic interactions does predict a critical linear suppression of the Curie-Weiss scale Θ for spin fluctuations as $t'_\perp \to t'^*_\perp$ [31,32], its slope [coefficient A of Eq. (27)] proves to be significantly larger than the one seen in experiments [80]. In this regard, we have found that adding a small $|\tilde{g}_{\rm ph}|$ is sufficient to reduce the downslope of Θ to values congruent with experiments [80], and this over a large range of retardation. This supports the view of an active role played by the electron-phonon interaction in the properties of the metallic state, especially those associated to quantum criticality at $t'^*_\perp$.

In this paper, we have dealt exclusively with the coupling of correlated electrons to low-energy acoustic phonons within the tight-binding scheme for the electronic structure, a coupling well known to be responsible for electronically driven structural instabilities in low-dimensional molecular materials [35,59]. We did not consider intramolecular (Holstein) phonon modes, also well known to be present. Their classification alongside their (small) coupling to electrons in $(TMTSF)_2X$ have been obtained from infrared optical studies [71]. These molecular phonons are characterized by relatively large energies and weak retardation effects compared to acoustic branches considered above. In first approximation, their influence can be incorporated through a redefinition of the nonretarded terms, amounting to a small and similar downward shift of the couplings g_i of the electron gas model. Since the latter couplings were taken as phenomenological constants whose range was fixed by experiments, the values taken in the present work should embody to some extent the influence of intramolecular phonons.

The interplay between electron-phonon and electron-electron interactions in the framework of the Holstein-Hubbard

model has been the subject of considerable attention in the past few years, especially in one dimension where, in the absence of interchain hopping and nesting alteration, SDW order is found to compete exclusively with a charge-density-wave state and, to a lesser degree, *s*-wave superconductivity when the phonon-mediated interaction strength is of the order of the direct Coulomb term [81–84].

In conclusion, we have performed a finite-temperature renormalization group analysis of the quasi-1D electron electron gas model with nonretarded electron-electron couplings and phonon-mediated interactions of the tight-binding electronic structure. For a phonon-mediated interaction that is weak compared to nonretarded terms, we found a reinforcement of antiferromagnetism and its transition toward superconductivity under bad nesting conditions of the electron spectrum. The weakness of phonon-mediated interactions acts as a decisive factor for the stability of antiferromagnetism against the Peierls phenomena in low-dimensional conductors. It is likely that these retarded interactions also have a built-in positive impact in the observation of organic superconductivity on the verge of antiferromagnetism in the Bechgaard salts.

ACKNOWLEDGMENTS

C.B. thanks the National Science and Engineering Research Council of Canada (NSERC) and the Réseau Québécois des Matériaux de Pointe (RQMP) for financial support. Computational resources were provided by the Réseau québécois de calcul de haute performance (RQCHP) and Compute Canada.

[1] O. Gurnnasson and O. Röuch, J. Phys.: Condens. Matter **20**, 043201 (2008).
[2] M. Capone, C. Castellani, and M. Grilli, Adv. Condens. Matter Phys. **2010**, 920860 (2010).
[3] J. J. Lee, F. T. Schmitt, R. G. Moore, S. Johnston, Y.-T. Cui, W. Li, M. Yi, Z. K. Liu, M. Hashimoto, Y. Zhang *et al.*, arXiv:1312.2633.
[4] C. Bourbonnais and D. Jérome, in *Physics of Organic Superconductors and Conductors*, Vol. 110, Springer Series in Materials Science, edited by A. G. Lebed (Springer, Heidelberg, 2008), pp. 357–412 .
[5] D. Jérome, A. Mazaud, M. Ribault, and K. Bechgaard, J. Phys. (Paris) Lett. **41**, L95 (1980).
[6] V. J. Emery, R. Bruinsma, and S. Barisic, Phys. Rev. Lett. **48**, 1039 (1982).
[7] V. J. Emery, Synth. Met. **13**, 21 (1986).
[8] L. G. Caron and C. Bourbonnais, Physica **143**, B453 (1986); C. Bourbonnais and L. G. Caron, Eur. Phys. Lett. **5**, 209 (1988).
[9] M. T. Béal-Monod, C. Bourbonnais, and V. J. Emery, Phys. Rev. B **34**, 7716 (1986).
[10] D. J. Scalapino, E. Loh, and J. E. Hirsch, Phys. Rev. B **34**, R8190 (1986).
[11] H. Shimahara, J. Phys. Soc. Jpn. **58**, 1735 (1989).
[12] S. Mazumdar, R. T. Clay, and D. K. Campbell, Phys. Rev. B **62**, 13400 (2000).
[13] K. Kuroki, R. Arita, and H. Aoki, Phys. Rev. B **63**, 094509 (2001).
[14] Y. Fuseya and Y. Suzumura, J. Phys. Soc. Jpn. **74**, 1263 (2005).
[15] Y. Fuseya, H. Kohno, and K. Miyake, J. Phys. Soc. Jpn. **74**, 722 (2005).
[16] J. Friedel, Eur. Phys. J. B **54**, 83 (2006).
[17] D. Jérome and H. J. Schulz, Adv. Phys. **31**, 299 (1982).
[18] L. J. Azevedo, J. E. Schirber, J. M. Williams, M. A. Beno, and D. R. Stephens, Phys. Rev. B **30**, 1570(R) (1984).
[19] T. Vuletic, P. Auban-Senzier, C. Pasquier, S. Tomic, D. Jerome, M. Heritier, and K. Bechgaard, Eur. Phys. J. B **25**, 319 (2002).
[20] N. Doiron-Leyraud, P. Auban-Senzier, S. René de Cotret, C. Bourbonnais, D. Jérome, K. Bechgaard, and L. Taillefer, Phys. Rev. B **80**, 214531 (2009).
[21] C. Bourbonnais, F. Creuzet, D. Jérome, K. Bechgaard, and A. Moradpour, J. Phys. (Paris) Lett. **45**, L755 (1984).
[22] F. Creuzet, C. Bourbonnais, L. G. Caron, D. Jérome, and A. Moradpour, Synth. Met. **19**, 277 (1987).
[23] W. Kang, S. T. Hannahs, and P. M. Chaikin, Phys. Rev. Lett. **70**, 3091 (1993).
[24] J. R. Cooper, W. Kang, P. Auban, G. Montambaux, D. Jerome, and K. Bechgaard, Phys. Rev. Lett. **63**, 1984 (1989).
[25] W. Wu, P. M. Chaikin, W. Kang, J. Shinagawa, W. Yu, and S. E. Brown, Phys. Rev. Lett. **94**, 097004 (2005).
[26] K. Yamaji, J. Phys. Soc. Jpn. **51**, 2787 (1982).
[27] H. Gutfreund, B. Horovitz, and M. Weger, J. Phys. (Paris) Coll. **44**, 983 (1983); B. Horovitz, H. Gutfreund, and M. Weger, Sol. State Comm. **39**, 541 (1981).
[28] Y. Hasegawa and H. Fukuyama, J. Phys. Soc. Jpn. **55**, 3978 (1986).
[29] R. Duprat and C. Bourbonnais, Eur. Phys. J. B **21**, 219 (2001).
[30] J. C. Nickel, R. Duprat, C. Bourbonnais and N. Dupuis, Phys. Rev. Lett. **95**, 247001 (2005); Phys. Rev. B **73**, 165126 (2006).
[31] C. Bourbonnais and A. Sedeki, Phys. Rev. B **80**, 085105 (2009).
[32] A. Sedeki, D. Bergeron, and C. Bourbonnais, Phys. Rev. B **85**, 165129 (2012).
[33] H. Meier, P. Auban-Senzier, C. Pépin, and D. Jérome, Phys. Rev. B **87**, 125128 (2013).
[34] J. Pouget, R. Moret, R. Comes, K. Bechgaard, J.-M. Fabre, and L. Giral, Mol. Cryst. Liq. Cryst. **79**, 129 (1982).
[35] J. P. Pouget, Crystals **2**, 466 (2012).
[36] V. J. Emery, J. Phys. (Paris) Coll. **44**, 977 (1983).
[37] H. Bakrim and C. Bourbonnais, Eur. Phys. Lett. **90**, 27001 (2010).
[38] A. Lanzara, P. V. Bogdanov, X. J. Zhou, S. Kellar, D. L. Feng, E. D. Lu, T. Yoshida, H. Eisaki, A. Fujimori, K. Kishiom *et al.*, Nature **412**, 510 (2001).
[39] G.-H. Gweon, T. Sasagawa, S. Y. Zhou, J. Graf, H. Takagi, D.-H. Lee, and A. Lanzara, Nature **430**, 187 (2004).
[40] H. Iwasawa, J. F. Douglas, K. Sato, T. Masui, Y. Yoshida, Z. Sun, H. Eisaki, H. Bando, A. Ino, M. Arita *et al.*, Phys. Rev. Lett. **101**, 157005 (2008).
[41] M. K. Crawford, M. N. Kunchur, W. E. Farneth, E. M. McCarron III, and S. J. Poon, Phys. Rev. B **41**, 282 (1990).
[42] J. Bauer and G. Sangiovanni, Phys. Rev. B **82**, 184535 (2010).
[43] F. D. Klironomos and S.-W. Tsai, Phys. Rev. B **74**, 205109 (2006).

[44] S.-W. Tsai, A. H. Castro Neto, R. Shankar, and D. K. Campbell, Phys. Rev. B **72**, 054531 (2005).
[45] G. Sangiovanni, M. Capone, C. Castellani, and M. Grilli, Phys. Rev. Lett. **94**, 026401 (2005).
[46] C. Honerkamp, H. C. Fu, and D.-H. Lee, Phys. Rev. B **75**, 014503 (2007).
[47] Z. B. Huang, W. Hanke, E. Arrigoni, and D. J. Scalapino, Phys. Rev. B **68**, 220507 (2003).
[48] A. W. Sandvik, D. J. Scalapino, and N. E. Bickers, Phys. Rev. B **69**, 094523 (2004).
[49] S. Andergassen, S. Caprara, C. Di Castro, and M. Grilli, Phys. Rev. Lett. **87**, 056401 (2001).
[50] N. Bulut and D. J. Scalapino, Phys. Rev. B **54**, 14971 (1996).
[51] J. Chang, E. Blackburn, A. T. Holmes, N. B. Christensen, J. Larsen, J. Mesot, R. Liang, D. A. Bonn, W. N. Hardy, A. Watenphul *et al.*, Nat. Phys. **8**, 871 (2012).
[52] M. L. Tacon, A. Bosak, M. Souliou, G. Dellea, T. Loew, R. Heid, K.-P. Bohnen, G. Ghiringhelli, M. Krisch, and B. Keimer, Nat. Phys. **10**, 52 (2014).
[53] P. M. Grant, Phys. Rev. B **26**, 6888 (1982).
[54] L. Ducasse, A. Abderraba, J. Hoarau, M. Pesquer, B. Gallois, and J. Gaultier, J. Phys. C **19**, 3805 (1986).
[55] D. L. Pévelen, J. Gaultier, Y. Barrans, D. Chassau, F. Castet, and L. Ducasse, Eur. Phys. J. B **19**, 363 (2001).
[56] J. Solyom, Adv. Phys. **28**, 201 (1979).
[57] V. J. Emery, in *Highly Conducting One-Dimensional Solids*, edited by J. T. Devreese, R. E. Evrard, and V. E. van Doren (Plenum, New York, 1979), p. 247.
[58] M. Ménard and C. Bourbonnais, Phys. Rev. B **83**, 075111 (2011).
[59] W. P. Su, J. R. Schrieffer and A. J. Heeger, Phys. Rev. B **22**, 2099 (1980); S. Barisic, *ibid.* **5**, 932 (1972).
[60] M. Krauzman, H. Poulet, and R. M. Pick, Phys. Rev. B **33**, 99 (1986).
[61] C. C. Homes and J. E. Eldridge, Phys. Rev. B **40**, 6138 (1989).
[62] J. P. Pouget, S. K. Khanna, F. Denoyer, R. Comès, A. F. Garito, and A. J. Heeger, Phys. Rev. Lett. **37**, 437 (1976).
[63] H. Bakrim and C. Bourbonnais, Phys. Rev. B **76**, 195115 (2007).
[64] Y. Hasegawa and H. Fukuyama, Physica B **143**, 447 (1986).
[65] G. Montambaux, Phys. Rev. B **38**, 4788 (1988).
[66] L. G. Caron and C. Bourbonnais, Phys. Rev. B **29**, 4230 (1984).
[67] P. A. Lee, T. M. Rice, and R. A. Klemm, Phys. Rev. B **15**, 2984 (1977).
[68] E. Fradkin and J. E. Hirsch, Phys. Rev. B. **27**, 1680 (1983).
[69] S. E. Brown, P. M. Chaikin, and M. J. Naughton, in *The Physics of Organic Superconductors and Conductors*, Vol. 110, Springer Series in Materials Science, edited by A. Lebed (Springer, Heidelberg, 2008), p. 49.
[70] Y. Kimura, M. Misawa, and A. Kawamoto, Phys. Rev. B **84**, 045123 (2011).
[71] D. Pedron, R. Bozio, M. Meneghetti, and C. Pecile, Phys. Rev. B **49**, 10893 (1994).
[72] F. Creuzet, C. Bourbonnais, L. G. Caron, D. Jérome, and K. Bechgaard, Synthetic Met. **19**, 289 (1987).
[73] L. G. Caron, F. Creuzet, P. Butaud, C. Bourbonnais, D. Jérocme, and K. Bechgaard, Synthetic Met. **27**, 123 (1988).
[74] D. S. Chow, P. Wzietek, D. Fogliatti, B. Alavi, D. J. Tantillo, C. A. Merlic, and S. E. Brown, Phys. Rev. Lett. **81**, 3984 (1998).
[75] H. Wilhelm, D. Jaccard, R. Duprat, C. Bourbonnais, D. Jérome, J. Moser, C. Carcel, and J. M. Fabre, Eur. Phys. J. B **21**, 175 (2001).
[76] T. Adachi, E. Ojima, K. Kato, H. Kobayashi, T. Miyazaki, M. Tokumoto, and A. Kobayashi, J. Am. Chem. Soc. **122**, 3238 (2000).
[77] J. Moser, M. Gabay, P. Auban-Senzier, D. Jérome, K. Bechgaard, and J. M. Fabre, Eur. Phys. J. B **1**, 39 (1998).
[78] P. Wzietek, F. Creuzet, C. Bourbonnais, D. Jérome, K. Bechgaard, and P. Batail, J. Phys. I (France) **3**, 171 (1993).
[79] J. Shinagawa, Y. Kurosaki, F. Zhang, C. Parker, S. E. Brown, D. Jérome, K. Bechgaard, and J. B. Christensen, Phys. Rev. Lett. **98**, 147002 (2007).
[80] C. Bourbonnais and A. Sedeki, C. R. Physique **12**, 532 (2011).
[81] R. P. Hardikar and R. T. Clay, Phys. Rev. B **75**, 245103 (2007).
[82] K.-M. Tam, S.-W. Tsai, D. K. Campbell, and A. H. Castro Neto, Phys. Rev. B **75**, 161103(R) (2007).
[83] J. Bauer, Eur. Phys. Lett. **90**, 27002 (2010).
[84] E. A. Nowadnick, S. Johnston, B. Moritz, R. T. Scalettar, and T. P. Devereaux, Phys. Rev. Lett. **109**, 246404 (2012).